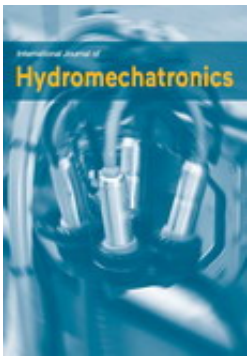


**International Journal of Hydromechatronics**

ISSN online: 2515-0472 - ISSN print: 2515-0464
https://www.inderscience.com/ijhm

# Hybrid model-driven and data-driven approach for the health assessment of axial piston pumps

Qun Chao, Zi Xu, Yuechen Shao, Jianfeng Tao, Chengliang Liu, Shuo Ding

**DOI:** 10.1504/IJHM.2022.10050130

**Article History:**

| | |
|---|---|
| Received: | 13 March 2022 |
| Accepted: | 11 July 2022 |
| Published online: | 21 February 2023 |

# Hybrid model-driven and data-driven approach for the health assessment of axial piston pumps

Qun Chao*

State Key Laboratory of Mechanical System and Vibration,
Shanghai Jiao Tong University,
Shanghai 200240, China
and
State Key Laboratory of Fluid Power and Mechatronic Systems,
Zhejiang University,
Hangzhou 310027, China
Email: chaoqun@sjtu.edu.cn
and
MoE Key Lab of Artificial Intelligence, AI Institute,
Shanghai Jiao Tong University,
Shanghai 200240, China
*Corresponding author

Zi Xu and Yuechen Shao

State Key Laboratory of Mechanical System and Vibration,
Shanghai Jiao Tong University,
Shanghai 200240, China
Email: waterxz@sjtu.edu.cn
Email: s-y-c-96@sjtu.edu.cn

Jianfeng Tao and Chengliang Liu

State Key Laboratory of Mechanical System and Vibration,
Shanghai Jiao Tong University,
Shanghai 200240, China
and
MoE Key Lab of Artificial Intelligence, AI Institute,
Shanghai Jiao Tong University,
Shanghai 200240, China
Email: jftao@sjtu.edu.cn
Email: chlliu@sjtu.edu.cn

Shuo Ding

Department of Biomedical Engineering,
National University of Singapore,
117583, Singapore
Email: bieding@nus.edu.sg

**Abstract:** Axial piston pumps are key components in hydraulic systems and their performance significantly affects the efficiency and reliability of hydraulic systems. Many data-driven approaches have been applied to the fault diagnosis of axial piston pumps. However, few studies focus on the performance degradation assessment that plays an important role in the predictive maintenance for axial piston pumps. This paper proposes a hybrid model-driven and data-driven approach to assess the health status of axial piston pumps. A physical flow loss model is established to solve for the flow loss coefficients of the axial piston pump under different operating conditions. The flow loss coefficients act as feature vectors to train a support vector data description (SVDD) model. A health indicator based on SVDD is put forward to quantitatively assess the pump health status. Experimental results under different pump health conditions confirm the effectiveness of the proposed method.

**Keywords:** axial piston pump; health assessment; model-driven; data-driven; support vector data description; SVDD.

**Reference** to this paper should be made as follows: Chao, Q., Xu, Z., Shao, Y., Tao, J., Liu, C. and Ding, S. (2023) 'Hybrid model-driven and data-driven approach for the health assessment of axial piston pumps', *Int. J. Hydromechatronics*, Vol. 6, No. 1, pp.76–92.

**Biographical notes:** Qun Chao received his BS in Mechanical Design Manufacturing and its Automation from Hefei University of Technology, Hefei, China in 2013, and PhD in Mechatronic Engineering from the State Key Laboratory of Fluid Power and Mechatronic Systems, Zhejiang University, Hangzhou, China in 2019. He worked as a Postdoctoral Fellow at Shanghai Jiao Tong University, Shanghai, China, from 2019 to 2022. He is currently an Associate Professor at the School of Mechanical Engineering, Shanghai Jiao Tong University. His main research interests are in smart hydraulic components and predictive maintenance of hydraulic systems.

Zi Xu received her BS degree from Beihang University, Beijing, China in 2019 and MS in Mechanical Engineering from Shanghai Jiao Tong University, Shanghai, China in 2022. Her research focuses on the fault diagnosis of axial piston pumps.

Yuechen Shao received his MS in Mechanical Engineering from Shanghai Jiao Tong University, Shanghai, China in 2021. He is currently a Doctoral student at the School of Mechanical Engineering, Shanghai Jiao Tong University. His research focuses on the condition monitoring of hydraulic systems.

Jianfeng Tao received his PhD degree in 2003 from School of Automation Science and Electrical Engineering, Beihang University. After postdoctoral positions at School of Mechanical Engineering, Shanghai Jiao Tong University, he joined Shanghai Jiao Tong University in 2006 and was promoted to an Associate Professor and Professor in 2013 and 2022, respectively. His research interests are in intelligent sensing and control of complex mechatronics systems, with particular attention to robotics system, construction machinery, and industrial fluid power transmission and control system.

Chengliang Liu received his PhD in Mechanical Engineering from Southeast University, Nanjing, China in 1999. He joined the Faculty of Shanghai Jiao Tong University as an Assistant Professor in the same year. In 2000, he was invited to work at University of Cincinnati and University of Wisconsin, respectively, as a senior visiting scholar. He was promoted to a Full Professor

in 2002, taking charge of Institute of Mechatronics. His research interests ranges from intelligent robot systems, precise agriculture network-based monitoring to GPS/GIS/RS-equipped apparatus/machinery.

Shuo Ding received his BS and PhD in Mechatronic Engineering from the State Key Laboratory of Fluid Power and Mechatronic Systems, Zhejiang University, Hangzhou, China in 2013 and 2019. From 2020, he works as a Research Fellow at National University of Singapore. His main research interests are in wearable robotics, exoskeleton and human-robot interaction.

## 1 Introduction

Axial piston pumps are widely used in industry applications, ranging from construction machinery and marine equipment to agricultural machinery and aerospace. They serve as the 'heart' of hydraulic systems to supply other hydraulic components with pressurised fluid by converting rotating mechanical energy into hydraulic power (Chao et al., 2022b). Their operational performance directly affects the efficiency and reliability of the overall hydraulic system. The faults and failures of axial piston pumps may lead to downtime of equipment with hydraulic systems and increase of maintenance costs, or even cause huge economic losses and catastrophic safety hazards. Therefore, it is urgent and necessary for axial piston pumps to perform an effective condition-based maintenance, so as to meet an ever increasing requirement on reliability and safety of hydraulic systems.

A well-scheduled condition-based maintenance greatly depends on the capability of fault detection and diagnosis. The fault detection aims to detect the failure occurrence as early as possible while the fault diagnosis attempts to identify the fault location and type as accurately as possible (Dai and Gao, 2013). During the last few decades, the fault diagnosis of axial piston pumps has been the subject of interest in hydraulic community. The fault diagnosis methods for axial piston pumps can be divided into three main categories (Dai and Gao, 2013): model-based, signal-based, and data-driven methods. The model-based method establishes mathematical models to assess the health status of axial piston pumps by identifying the physical parameters, such as leakage flow rate (Wiens and Fernandes, 2019) and discharge pressure ripple (Palazzolo et al., 2008). The signal-based method involves no complex physical model and it often uses signal processing techniques, such as time-domain analysis (Tang et al., 2021a), frequency-domain analysis (Wang et al., 2019; Gao et al., 2021) and time-frequency analysis (Wu et al., 2021), to extract features and detect symptoms related to the pump faults. The data-driven method usually employs machine learning algorithms, especially deep learning algorithms, to learn implicit knowledge from a huge amount of historic data. Many researchers have introduced deep learning algorithms into the fault diagnosis of axial piston pumps, including one-dimensional convolutional neural network (CNN) (Chao et al., 2020a) two-dimensional CNN (Chao et al., 2020b, 2022a; Tang et al., 2021b, 2022a, 2022b), long short term network (Wei et al., 2021), and generative adversarial network (Jiang et al., 2021).

A thorough overview of the current literature shows that deep learning methods have achieved impressive diagnostic performance in the field of axial piston pumps. However, the majority of previous studies focused on the fault classification of axial piston pumps and few studies have been done on their health assessment. For the condition monitoring

of axial piston pumps, the health assessment should deserve more attention than the fault classification in practical applications. This is because:

a the health assessment enables one to take preventive measures to avoid pump failure as early as possible by monitoring the pump performance degradation

b it offers quantitative basis for making maintenance decisions.

Therefore, this paper proposes a hybrid model-driven and data-driven method to assess the health status of axial piston pumps. First, the flow loss model for axial piston pumps is developed to solve for the flow loss coefficients. Then, these flow loss coefficients are fed into a support vector data description (SVDD) model to calculate the pump health index. Finally, experiments are performed on an axial piston pump operating under different health conditions to validate the proposed health assessment method.

## 2 Machine description

Figure 1 shows a cross-sectional view of a swash-plate type axial piston pump. The working parts of the pump are enclosed in a sealed housing and end cover, among which the rotating kits are supported by two tapered roller bearings at shaft ends. The cylinder block accommodates an odd number of pistons in a circular array at equal intervals about its centreline. A ball-and-socket joint connects each pair of piston to a slipper, which allows the slipper to rotate around the piston ball. The slippers are held against the inclined swash plate while the cylinder block is held against the stationary valve plate. The spring nested in the cylinder block provides a preload on the retainer (through a set of pins and a ball guide) and cylinder block to keep a reasonable clearance between the slippers and swash plate and between the cylinder block and valve plate. The shaft drives the cylinder block together with the piston-slipper assemblies to rotate against the valve plate, during which the slippers slide on the swash plate and force the pistons to reciprocate in the cylinder bores. In the meantime, variable displacement chamber volumes form between the cylinder bores and pistons. The displacement chamber volumes increase to receive low-pressure fluid through one opening in the valve plate when the pistons are pulled out of the cylinder bores. Alternatively, the displacement chamber volumes decrease to discharge high-pressure fluid through the other opening in the valve plate when the pistons are pushed into the cylinder bores. As a result, the combined effect of all displacement chambers produces a continuous delivery flow. The volumetric displacement of the pump can be regulated by adjusting the swash-plate angle through the control valve and variable piston.

Three main lubricating interfaces form between movable parts in the axial piston pump, including the slipper/swash plate interface, the piston/cylinder block interface, and the cylinder block/valve plate interface. These lubricating interfaces are key design elements for axial piston pumps. They act as sliding bearing and gap sealing between movable parts and represent the sources of leakage from the displacement chambers to the pump housing. The wear of lubricating interfaces is one of main failure modes for axial piston pumps, especially the abrasive wear due to fluid contamination. The worn lubricating interfaces increase the gap height between movable parts, and thus increasing leakage flow of axial piston pumps.

**Figure 1** Cross-section of a swash-plate type axial piston pump

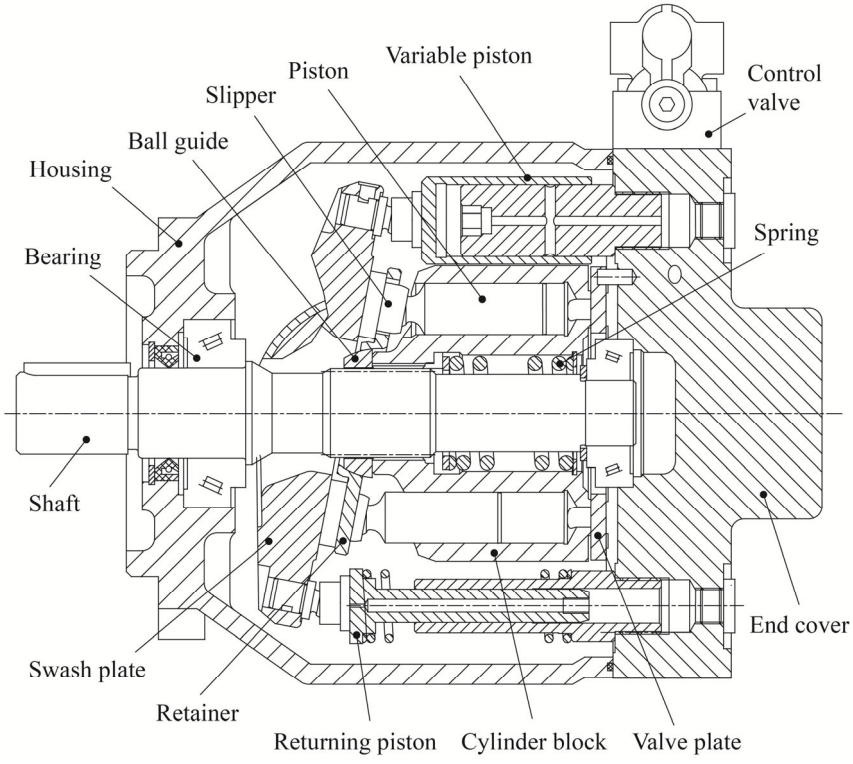


## 3 The proposed method

The delivery flow rate of an axial piston pump is influenced not only by the health status, but also by the operating conditions including inlet and outlet pressures, rotational speed, volumetric displacement, and fluid temperature. This means that the reduction in delivery flow rate may result from increased outlet pressure rather than increased gap height due to wear. In this case, it is critical to find an indicator independent of operating conditions to reflect the health status of axial piston pumps. The flow loss coefficients are a function of the geometrical dimensions of axial piston pumps and can reflect their wear conditions. Specifically, the wear of movable parts will increase gap height and leakage flow in the lubricating interfaces. Moreover, the flow loss coefficients of axial piston pumps are almost unaffected by operating conditions. Therefore, they can represent the pump's flow losses due to lubricating interface wear even under variable operating conditions.

Figure 2 illustrates how the proposed method assesses the health status of axial piston pumps. The basic idea behind the proposed method is to compare the feature distributions between healthy and monitored pumps. In the first step, healthy signals are collected at different operating points, including inlet and output pressures, oil temperature, rotational speed, and delivery flow rate. The flow loss equation uses these healthy signals to solve for a set of flow loss coefficients. The flow loss coefficients act as feature vectors to train

a SVDD model, generating an optimal decision hypersphere under healthy condition. In the second step, the testing signals are collected from the monitored pump in a similar way and their feature distances relative to the hypersphere centre are calculated. Finally, each feature distance is transformed into a health index ranging from 0 to 1.0, where higher health index represents more healthy status of the pump.

**Figure 2** Flowchart of the proposed method for health assessment of axial piston pumps (see online version for colours)

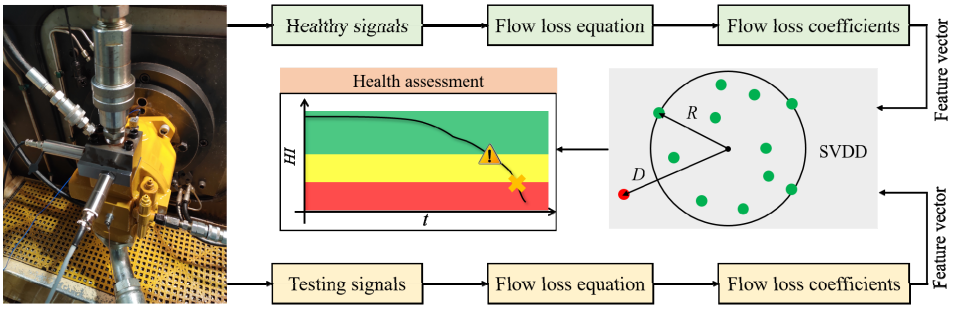


## *3.1 Flow loss model*

The performance degradation of axial piston pumps can be reflected by their flow losses (Geng et al., 2021). The flow losses of an axial piston pump consist of compression loss and leakage loss, where the latter flow loss can be subdivided into laminar leakage loss and turbulent leakage loss (Mettakadapa et al., 2015). The compression loss occurs in the displacement chambers due to fluid compressibility and periodic switch between high and low pressure sides. The leakage loss mainly occurs in the lubricating interfaces.

The total flow loss of an axial piston pump can be determined by the difference between ideal and actual delivery flow rates (Manring, 2016; Załuski, 2022).

$$\omega V_g - Q = \kappa_1' \frac{\omega \Delta p}{\beta} + \kappa_2' \frac{\Delta p}{\mu} + \kappa_3' \sqrt{\frac{\Delta p}{\rho}} \tag{1}$$

where $\omega$ is the rotational speed, $V_g$ is the volumetric displacement, $Q$ is the actual delivery flow rate, $\Delta p$ is the pressure difference between outlet and case drain ports, $\mu$ is the fluid dynamic viscosity, $\rho$ is the fluid density, $\beta$ is the fluid bulk modulus, $\kappa_1'$, $\kappa_2'$, $\kappa_3'$, and are the respective coefficients of compression loss, laminar leakage, and turbulent leakage.

To obtain dimensionless flow loss coefficients, equation (1) is rewritten as

$$\begin{aligned} \omega V_g - Q &= \frac{\kappa_1'}{V_g} \frac{\omega V_g \Delta p}{\beta} + \frac{\kappa_2'}{V_g} \frac{V_g \Delta p}{\mu} + \frac{\kappa_3'}{V_g^{2/3}} V_g^{2/3} \sqrt{\frac{\Delta p}{\rho}} \\ &= \kappa_1 \frac{\omega V_g \Delta p}{\beta} + \kappa_2 \frac{V_g \Delta p}{\mu} + \kappa_3 V_g^{2/3} \sqrt{\frac{\Delta p}{\rho}} \end{aligned} \tag{2}$$

Assume that a total of $n$ groups of measurement data are available. The flow loss coefficients in equation (2) can be solved by the following matrix function (Manring, 2016):

$$\underbrace{\begin{bmatrix} \omega_1 V_{g1}\Delta p_1/\beta & V_{g1}\Delta p_1/\mu_1 & V_{g1}^{2/3}\sqrt{\Delta p_1/\rho} \\ \omega_2 V_{g2}\Delta p_2/\beta & V_{g2}\Delta p_2/\mu_2 & V_{g2}^{2/3}\sqrt{\Delta p_2/\rho} \\ \vdots & \vdots & \vdots \\ \omega_n V_{gn}\Delta p_n/\beta & V_{gn}\Delta p_n/\mu_n & V_{gn}^{2/3}\sqrt{\Delta p_n/\rho} \end{bmatrix}}_{P} \underbrace{\begin{bmatrix} \kappa_1 \\ \kappa_2 \\ \kappa_3 \end{bmatrix}}_{K} = \underbrace{\begin{bmatrix} \omega_1 V_{g1} - Q_1 \\ \omega_2 V_{g2} - Q_2 \\ \vdots \\ \omega_n V_{gn} - Q_n \end{bmatrix}}_{Q} \tag{3}$$

The fluid dynamic viscosity at certain temperature in equation (3) can be empirically expressed by Geng et al. (2021)

$$\mu = \mu_0 \exp\left(c_1 p - c_2 \Delta T\right) \tag{4}$$

where $\mu_0$ is the reference dynamic viscosity, $p$ is the fluid pressure, $\Delta T$ is the increase in fluid temperature, $c_1$ is the pressure coefficient of 0.02, and $c_2$ is the temperature coefficient of 0.03.

Each row in matrix $\boldsymbol{P}$ and column vector $\boldsymbol{Q}$ represents a group of measurement data. The column vector $\boldsymbol{K}$ containing flow loss coefficients is the only unknown variable in equation (3). Equation (3) involves a typical multivariate linear regression and the analytical solution of K can be obtained by least square method.

$$\boldsymbol{K} = (\boldsymbol{P}^{\mathrm{T}}\boldsymbol{P})^{-1}\boldsymbol{P}^{\mathrm{T}}\boldsymbol{Q} \tag{5}$$

### *3.2 Support vector data description*

SVDD a typical one-class classification method, which was first developed by Tax and Duin (1999, 2004). Compared with other classification methods, it does not need to assume the probability distribution of target data (Cha et al., 2014). SVDD has been widely used in novelty detection (Wang et al., 2013), fault diagnosis (Duan et al., 2016), and health assessment (Zhang et al., 2021).

The training process of SVDD is to find a set of support vectors determining an optimal hypersphere boundary of the target data in feature space. The enclosed hypersphere with centre a and radius R should contain the training samples within its minimum volume (i.e., minimum radius). This is a constrained optimisation problem that can be defined as

$$\begin{aligned} &\min_{a,R,\zeta_i} R^2 + C\sum_{i=1}^{N}\zeta_i \\ &s.t.\ \ \left\|x_i - a\right\|^2 \le R^2 + \zeta_i,\ \zeta_i \ge 0,\ i = 1,\ 2,\ ...,\ N \end{aligned} \tag{6}$$

where $x_i$ is the $i^{\text{th}}$ sample vector from the training dataset, $N$ is the total number of training samples, $\zeta_i$ is the slack variable of the $i^{\text{th}}$ sample vector, and $C$ is the penalty factor.

The constrained optimisation problem in equation (6) can be transformed into an unconstrained counterpart by Lagrange multiplier approach.

$$\min_{a,R,\zeta_i} \max_{\lambda_i,\gamma_i} R^2 + C\sum_{i=1}^{N}\zeta_i + \sum_{i=1}^{N}\lambda_i\left(\|x_i - a\|^2 - R^2 - \zeta_i\right) - \sum_{i=1}^{N}\gamma_i\zeta_i \tag{7}$$

where $\lambda_i \geq 0$ and $\gamma_i \geq 0$ are the Lagrange multipliers.

Solving equation (7) yields the hypersphere centre as follows:

$$\boldsymbol{a} = \sum_{i=1}^{N}\lambda_i \boldsymbol{x}_i \tag{8}$$

The hypersphere radius can be determined by the distance between one of support vectors $x_v$ and the hypersphere centre.

$$R = \sqrt{\|\boldsymbol{x}_v - \boldsymbol{a}\|^2} = \sqrt{\boldsymbol{x}_v \cdot \boldsymbol{x}_v - 2\sum_{i=1}^{N}\lambda_i \boldsymbol{x}_v \cdot \boldsymbol{x}_i + \sum_{i=1}^{N}\sum_{j=1}^{N}\lambda_i\lambda_j\left(\boldsymbol{x}_i \cdot \boldsymbol{x}_j\right)} \tag{9}$$

For a test sample vector $\boldsymbol{x}_t$, its distance $D$ relative to the hypersphere centre is given by

$$D = \sqrt{\|\boldsymbol{x}_t - \boldsymbol{a}\|^2} = \sqrt{\boldsymbol{x}_t \cdot \boldsymbol{x}_t - 2\sum_{i=1}^{N}\lambda_i \boldsymbol{x}_t \cdot \boldsymbol{x}_i + \sum_{i=1}^{N}\sum_{j=1}^{N}\lambda_i\lambda_j\left(\boldsymbol{x}_i \cdot \boldsymbol{x}_j\right)} \tag{10}$$

This work adopts the Gaussian RBF kernel as the kernel function to calculate the dot products in equations (9) and (10).

$$K(\boldsymbol{x}, \boldsymbol{z}) = \varphi(\boldsymbol{x}) \cdot \varphi(\boldsymbol{z}) = \exp\left(-\frac{1}{2}\|\boldsymbol{x} - \boldsymbol{z}\|\right) \tag{11}$$

where $K(\cdot, \cdot)$ represents the kernel function and $\varphi(\cdot)$ represents an implicit function mapping the data in input space into a higher-dimensional feature space.

Recognising that $K(\boldsymbol{x}_v, \boldsymbol{x}_v) = K(\boldsymbol{x}_t, \boldsymbol{x}_t) = 1$, equations (9) and (10) can be rewritten as

$$R = \sqrt{1 - 2\sum_{i=1}^{N}\lambda_i K\left(\boldsymbol{x}_v, \boldsymbol{x}_i\right) + \sum_{i=1}^{N}\sum_{j=1}^{N}\lambda_i\lambda_j K\left(\boldsymbol{x}_i, \boldsymbol{x}_j\right)} \tag{12}$$

$$D = \sqrt{1 - 2\sum_{i=1}^{N}\lambda_i K\left(\boldsymbol{x}_t, \boldsymbol{x}_i\right) + \sum_{i=1}^{N}\sum_{j=1}^{N}\lambda_i\lambda_j K\left(\boldsymbol{x}_i, \boldsymbol{x}_j\right)} \tag{13}$$

### *3.3 Health index*

To represent the health status of axial piston pumps, a dimensionless health index (HI) is constructed based on the distance from the hypersphere centre to the test sample.

$$HI = \frac{2}{1 + \exp\left(\alpha\left\|\varphi\left(\boldsymbol{x}_t\right) - \boldsymbol{a}\right\|\right)} \tag{14}$$

where $\alpha$ is a positive degradation factor that controls the sensibility of *HI* to the pump performance degradation.

Equation (14) suggests that the *HI* ranges from 0 to 1 and the maximum value of 1 indicates a perfectly healthy condition for the monitored pump. The *HI* increases when

the test sample approaches the hypersphere centre. It achieves the maximum value of 1 when the test sample is located at the hypersphere centre.

## 4 Experimental investigation

To validate the proposed health assessment method, experiments were carried out on an open-circuit swash-plate type axial piston pump (L10VSO71) by a hydraulic test rig, as shown in Figure 3. The electric motor drove the tested pump to receive hydraulic oil from the charge pump. The heater kept the temperature of supplied hydraulic oil at 50 ± 2℃ during the pump operation. The inlet pressure of the tested pump was controlled at 1.6 ± 0.1 bar by a proportional relief valve. The load on the tested pump was simulated by another proportional relief valve. Several sensors were used to monitor the pump conditions. The torque/speed sensor measured the rotational speed and input torque of the pump shaft. Two pressure sensors were separately installed at the inlet and outlet lines to measure the pump's inlet and outlet pressures. In addition, two flow metres were separately mounted at the outlet and drainage lines to record the delivery and leakage flow rates. A temperature sensor was used to monitor the temperature of supplied hydraulic oil.

Experimental data were collected when the tested pump operated at a full displacement but at different rotational speeds and outlet pressures. Specifically, the rotational speed increased from 500 r/min to 2,000 r/min with an increment of 500 r/min and the outlet pressure increased from 5 MPa to 20 MPa with an increment of 5 MPa. Therefore, there were a total of 16 operating points for the tested pump. The control unit was responsible for implementing various combinations of rotational speed and outlet pressure. At each operating point, the data acquisition unit collected monitoring signals for 30 s at a sampling frequency of 1000 Hz, including the rotational speed, input torque, inlet and outlet pressures, delivery and leakage flow rates, and oil temperature.

The pump was tested under healthy and faulty conditions. The faulty cases were created by intentionally assembling one or more defective pistons inside the pump. Compared with normal piston Figure 4(a), the defective piston Figure 4(b) had three artificial scratches on the contact surface along the axial direction, which were distributed uniformly in the circumferential direction. The scratches were obtained by an electro discharge machining operation and each of them were 0.2 mm in both width and depth.

The dataset were collected at four different levels of pump health status by replacing normal pistons with defective ones. Figure 5 illustrates the layout of normal and defective pistons in the cylinder block for each health status, where more defective pistons means worse pump health status. The tested pump was first equipped with nine normal pistons Figure 5(a) and the healthy data were collected at 16 operating points. After that, the tested pump was disassembled and one of its normal pistons was replaced by a defective piston Figure 5(b). The data were collected from the faulty pump equipped with one defective piston under the same operating conditions. Similarly, we obtained datasets from the faulty pump equipped with four defective pistons Figure 5(c) and nine defective pistons Figure 5(d), respectively. Figure 6 shows an overall view of the rotating group of the faulty pump containing nine defective pistons.

**Figure 3** (a) Hydraulic circuit schematic (b) Test rig for axial piston pumps (see online version for colours)

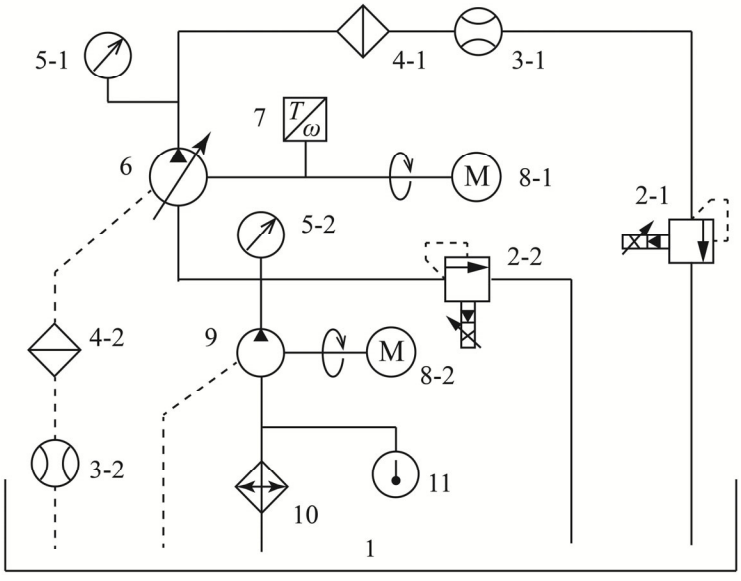


1 Tank 2 Proportional relief valve 3 Flow meter 4 Filter 5 Pressure sensor
6 Tested pump 7 Torque/speed sensor 8 Electric motor 9 Charge pump
10 Heater 11 Temperature sensor

(a)


(b)

**Figure 4** Comparison between (a) normal piston and (b) faulty piston for the tested pump (see online version for colours)

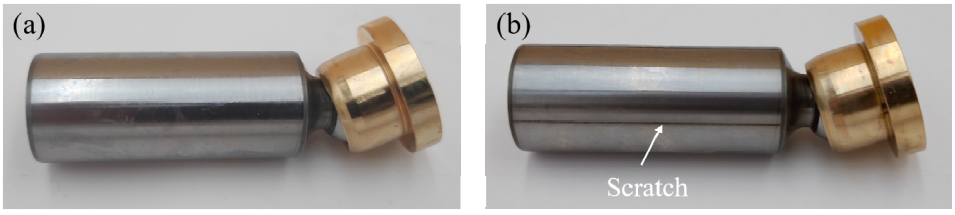


**Figure 5** Layout of healthy and defective pistons in the cylinder block: (a) all nine normal pistons; (b) one defective piston; (c) four defective pistons; (d) all nine defective pistons (see online version for colours)

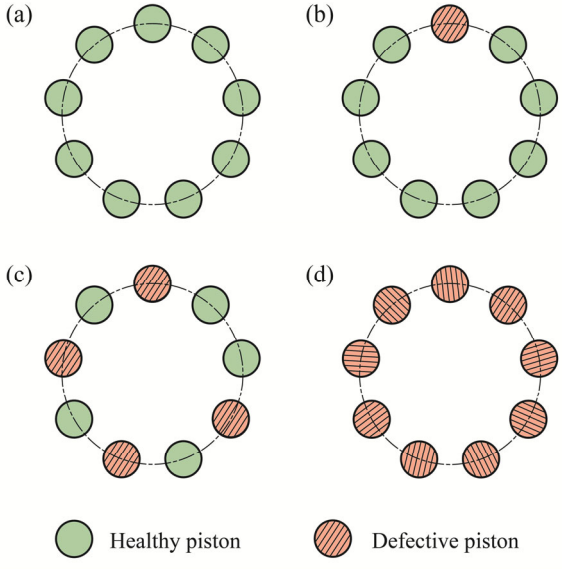


**Figure 6** Rotating group of the faulty pump containing nine defective pistons (see online version for colours)

## 5 Results and discussion

Figure 7 presents an example of discharge flow rates for different levels of pump health status at an outlet pressure of 20 MPa and a rotational speed of 1000 r/min. More defective pistons represent more serious degradation of pump performance. The fluctuant discharge flow (also called kinematic flow ripple) arises from the combined effects of a finite number of pistons that periodically communicate with the suction and discharge ports of the valve plate. It can be observed in Figure 7 that the discharge flow rate decreases with the number of defective pistons assembled into the tested pump. This is mainly because the defective pistons increase the gap height in piston/cylinder block interfaces and thus increasing the leakage flow rates, as shown in Figure 8. Compared with the healthy pump, the leakage flow rate of faulty pump rises by 11.7%, 23.5%, and 59.3%, respectively, when the number of defective pistons increases to one, four, and nine.

Table 1 summarises the average and standard deviation of the monitoring parameters at an outlet pressure of 20 MPa and a rotational speed of 1000 r/min. For each level of health status, the average discharge pressure and rotational speed are close to 20 MPa and 1000 r/min, respectively, and their small standard deviations suggest a steady state of the operating pump. The oil temperature is kept around 50°C for each level of health status to reduce the temperature effects on the flow characteristics. As expected, more defective pistons lead to larger average leakage flow rate and thus smaller average delivery flow rate. In addition, the healthy pump has a smaller standard deviation of delivery flow rate than faulty pumps, which indicates that defective pistons increase the discharge flow ripple. This finding corresponds to the waveform results in Figure 7, where the healthy pump experiences a smaller fluctuation of discharge flow than faulty pumps. By contrast, Table 1 and Figure 8 show that the fluctuation of leakage flow appears to be less sensitive to the degradation of pump performance.

**Figure 7** Discharge flow rates for different levels of health status (outlet pressure = 20 MPa, rotational speed = 1,000 r/min) (see online version for colours)

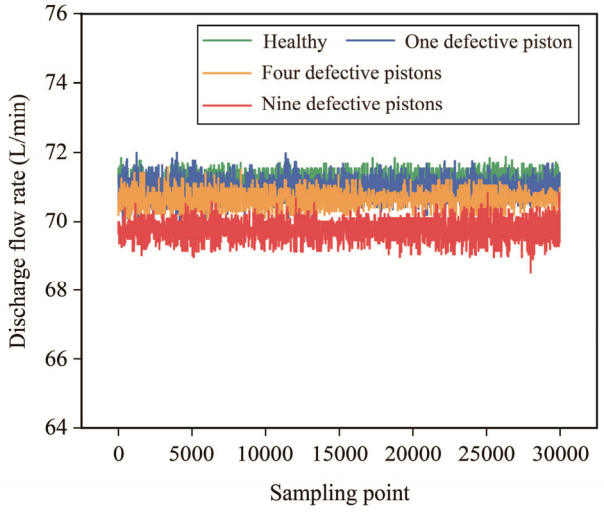

**Figure 8** Leakage flow rates for different levels of pump health status (outlet pressure = 20 MPa, rotational speed = 1,000 r/min) (see online version for colours)

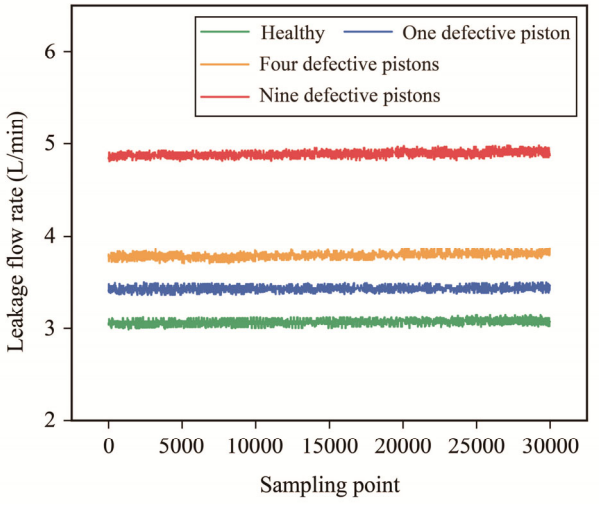


Table 2 compares the flow loss coefficients between four levels of pump health status under the same operating conditions. Each flow loss coefficient increases with the number of defective pistons. Among the three flow loss coefficients, the one associated with the laminar leakage is larger than the other two flow loss coefficients. This can be explained by the fact that the flow losses in the axial piston pump are dominated by the laminar leakage (Nie et al., 2021; Kroneis et al., 2022). The flow loss coefficient of laminar leakage is also found to be most sensitive to the pump performance degradation. This founding agrees with the experimental design because the artificial scratches on the piston increase the laminar leakage by increasing local fluid film thickness between the piston and cylinder block. The comparison of each flow loss coefficient between different levels of health status shows that the flow loss coefficient is less sensitive to the incipient performance degradation. In other words, the increase in flow loss coefficient may be too small to be detected by the SVDD model when the tested pump has only one defective piston.

**Table 1** Measured parameters under steady operating conditions for different levels of pump health status (outlet pressure = 20 MPa, rotational speed = 1000 r/min)

| *Level of health status* | *Delivery flow rate (L/min)* | *Leakage flow rate (L/min)* | *Rotational speed (r/min)* | *Discharge pressure (MPa)* | *Oil temperature (℃)* |
|---|---|---|---|---|---|
| Healthy | 71.2 ± 0.23 | 3.07 ± 0.03 | 1000 ± 1 | 19.6 ± 0.2 | 49.6 ± 0.2 |
| One defective piston | 70.9 ± 0.32 | 3.43 ± 0.03 | 1000 ± 1 | 20.2 ± 0.4 | 48.9 ± 0.4 |
| Four defective pistons | 70.7 ± 0.25 | 3.79 ± 0.03 | 1000 ± 1 | 19.8 ± 0.3 | 49.8 ± 0.4 |
| All nine defective pistons | 69.7 ± 0.31 | 4.89 ± 0.03 | 1000 ± 1 | 20.1 ± 0.4 | 49.5 ± 0.4 |

**Table 2** An example of flow loss coefficients for different levels of pump health status

| *Level of health status* | $\kappa_1$ | $\kappa_2$ | $\kappa_3$ |
|---|---|---|---|
| Healthy | $1.95 \times 10^{-17}$ | $8.85 \times 10^{-9}$ | $6.69 \times 10^{-18}$ |
| One defective piston | $1.97 \times 10^{-17}$ | $8.95 \times 10^{-9}$ | $6.74 \times 10^{-18}$ |
| Four defective pistons | $2.15 \times 10^{-17}$ | $9.78 \times 10^{-9}$ | $7.36 \times 10^{-18}$ |
| All nine defective pistons | $2.51 \times 10^{-17}$ | $11.36 \times 10^{-9}$ | $8.57 \times 10^{-18}$ |

In practical industrial applications, healthy data are more readily available for axial piston pumps than faulty data. Therefore, the SVDD model is first trained by healthy data and then tested by data from four levels of health status, as shown in Table 3. The healthy data are divided into two parts and they serve as training and testing datasets, respectively. Each sample fed to the SVDD model represents a group of flow loss coefficients that have been solved by the flow loss equations.

Figure 9 compares the feature distances of testing samples relative to the hypersphere centre between different levels of pump health status. It can be seen that the feature distance becomes greater when the tested pump contains more defective pistons. This means that the testing samples run away from the hypersphere centre in the high-dimensional feature space when the pump performance degrades. Therefore, the feature distance of test samples can be used to represent the health status of the monitored pump.

**Table 3** Sample numbers of training and testing dataset

| *Training dataset* | *Testing dataset* | | | |
|---|---|---|---|---|
| *Healthy* | *Healthy* | *One defective piston* | *Four defective pistons* | *All nine defective pistons* |
| 50 | 50 | 50 | 50 | 50 |

**Figure 9** Feature distances of the testing samples relative to the hypersphere centre (see online version for colours)

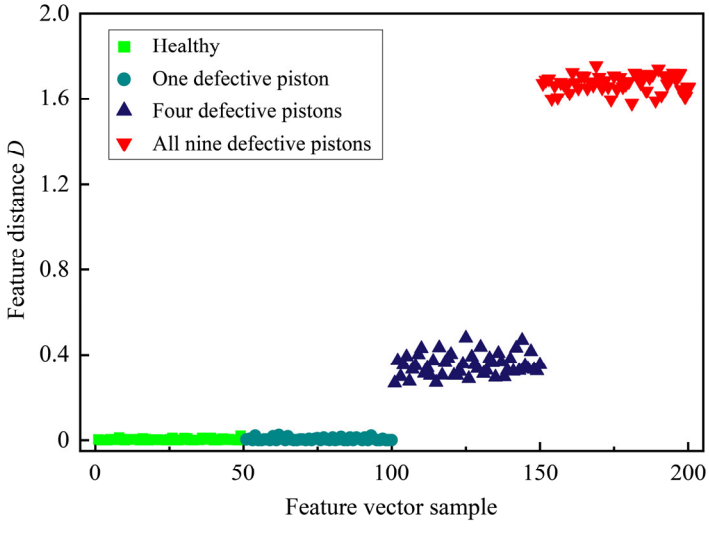

Figure 10 presents the *HI* for different levels of pump health status, where the *HI* is transformed from the feature distance of test samples with respect to the hypersphere centre, as shown in equation (14). As expected, the *HI* becomes lower as the distance of feature vectors increases due to pump performance degradation. The *HI* significantly drops when the monitored pump experiences an obvious performance degradation (i.e., four or nine defective pistons) but it hardly identifies the incipient performance degradation (i.e., one defective piston).

There are two possible reasons for the low sensitivity of *HI* to the incipient performance degradation of axial piston pumps. First, the external leakage flow of axial piston pumps is too small to be detected at their initial stage of performance degradation. Second, the flow signal responds slowly to the pump health state due to the poor frequency response characteristics of flow metres. Therefore, additional high-frequency signals, such as outlet pressure and housing vibration, may be required to monitor the health status of axial piston pumps.

**Figure 10** Calculated *HI* for different levels of pump health status (see online version for colours)

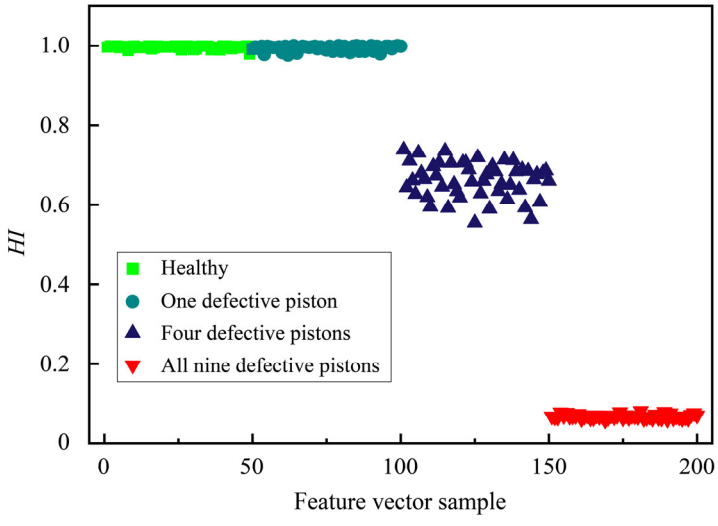


## 6 Conclusions

This paper proposes a hybrid model-driven and data-driven approach for the health assessment of axial piston pumps. A flow loss model of axial piston pumps is developed to solve for flow loss coefficients that form feature vectors with explicit physical meanings. The SVDD based machine learning model receives these feature vectors to quantitatively evaluate the difference between healthy and faulty data, which will be transformed into a health index ranging from 0 to 1. The experimental results show a promising prospect of the proposed method in the health assessment of axial piston pumps. On the other hand, it remains a challenge for the present method to detect the incipient performance degradation of axial piston pumps. The future work may address this challenge from two aspects. First, the input feature vector integrates high-frequency

signals, such as discharge pressure ripple and housing vibration. Second, improved versions of the standard SVDD model can be developed, such as density weighted SVDD model.

## Acknowledgements

This work was supported by the National Key R&D Program of China (No. 2018YFB1702503), the Open Foundation of the State Key Laboratory of Fluid Power and Mechatronic Systems (No. GZKF-202108), and the Ministry of Education-China Mobile Research Foundation (No. MCM20180703). The authors are thankful to Liyuan Hydraulic (Suzhou) Co., Ltd. for the help in preparing the experiments of this work.

## References

Cha, M., Kim, J.S. and Baek, J.G. (2014) 'Density weighted support vector data description', *Expert Systems with Applications*, Vol. 41, No. 7, pp.3343–3350.

Chao, Q., Tao, J., Wei, X. et al. (2020a) 'Cavitation intensity recognition for high-speed axial piston pumps using 1-D convolutional neural networks with multi-channel inputs of vibration signals', *Alexandria Engineering Journal*, Vol. 59, No. 6, pp.4463–4473.

Chao, Q., Tao, J., Wei, X. et al. (2020b) 'Identification of cavitation intensity for high-speed aviation hydraulic pumps using 2D convolutional neural networks with an input of RGB-based vibration data', Measurement Science and Technology, Vol. 31, No. 10, p.105102.

Chao, Q., Gao, H., Tao, J. et al. (2022a) 'Adaptive decision-level fusion strategy for the fault diagnosis of axial piston pumps using multiple channels of vibration signals', *Science China Technological Sciences*, Vol. 65, No. 2, pp.470–480.

Chao, Q., Zhang, J., Xu, B. et al. (2022b) 'Integrated slipper retainer mechanism to eliminate slipper wear in high-speed axial piston pumps', *Frontiers of Mechanical Engineering*, Vol. 17, No. 1, p.1.

Dai. X. and Gao, Z. (2013) 'From model, signal to knowledge: A data-driven perspective of fault detection and diagnosis', *IEEE Transactions on Industrial Informatics*, Vol. 9, No. 4, pp.2226–2238.

Duan, L., Xie, M., Bai, T. et al. (2016) 'A new support vector data description method for machinery fault diagnosis with unbalanced datasets', *Expert Systems with Applications*, Vol. 64, pp.239–246.

Gao, Q., Xiang, J., Hou, S. et al (2021) 'Method using L-kurtosis and enhanced clustering-based segmentation to detect faults in axial piston pumps', *Mechanical Systems and Signal Processing*, Vol. 147, p.107130.

Geng, B., Gu, L., Liu, J. et al. (2021) 'Dynamic modeling of fluid nonlinear compression loss and flow loss oriented to fault diagnosis of axial piston pump', *Proceedings of the Institution of Mechanical Engineers, Part C: Journal of Mechanical Engineering Science*, Vol. 235, No. 17, pp.3236–3251.

Jiang, W., Wang, C., Zou, J. et al. (2021) 'Application of deep learning in fault diagnosis of rotating machinery', *Processes*, Vol. 9, No. 6, p.919.

Kroneis, M., Scheerer, R., Bobach, L. et al. (2022) 'Validation of a coupled multibody and TEHL simulation by a piston/cylinder component test rig', *Proceedings of the Institution of Mechanical Engineers, Part J: Journal of Engineering Tribology.*

Manring, N.D. (2016) 'Mapping the efficiency for a hydrostatic transmission', *Journal of Dynamic Systems, Measurement and Control*, Vol. 138, No. 3, p.31004.

Mettakadapa, S., Bair, S., Aoki, S. et al. (2015) 'A fluid property model for piston pump case drain and pressure compensator flow losses', in *Proceedings of the ASME/BATH 2015 Symposium on Fluid Power and Motion Control*, Chicago, USA, V001T01A009.

Nie, S., Guo, M., Yin, F. et al. (2021) 'Research on fluid-structure interaction for piston/cylinder tribopair of seawater hydraulic axial piston pump in deep-sea environment', *Ocean Engineering*, Vol. 219, p.108222.

Palazzolo, J.J., Scheunemann, L.D. and Hartin, J.R. (2008) 'Leakage fault detection method for axial-piston variable displacement pumps', in *2008 IEEE Aerospace Conference*, Big Sky, USA.

Tang, H., Fu, Z. and Huang, Y. (2021a) 'A fault diagnosis method for loose slipper failure of piston pump in construction machinery under changing load', *Applied Acoustics*, Vol. 172, p.107634.

Tang, S., Zhu, Y. and Yuan, S. (2021b) 'An improved convolutional neural network with an adaptable learning rate towards multi-signal fault diagnosis of hydraulic piston pump', *Advanced Engineering Informatics*, Vol. 50, p.101406.

Tang, S., Zhu, Y. and Yuan, S. (2022a) 'Intelligent fault diagnosis of hydraulic piston pump based on deep learning and Bayesian optimization', *ISA Transactions*, https://doi.org/10.1016/J.ISATRA.2022.01.013.

Tang, S., Zhu, Y. and Yuan, S. (2022b) 'A novel adaptive convolutional neural network for fault diagnosis of hydraulic piston pump with acoustic images', *Advanced Engineering Informatics*, Vol. 52, p.101554.

Tax, D.M.J. and Duin, R.P.W. (1999) 'Support vector domain description', *Pattern Recognition Letter*s, Vol. 20, Nos. 11–13, pp.1191–1199.

Tax, D.M.J. and Duin, R.P.W. (2004) 'Support vector data description', *Machine Learning*, Vol. 54, pp.45–66.

Wang, S., Xiang, J. and Tang, H. et al (2019) 'Minimum entropy deconvolution based on simulation-determined band pass filter to detect faults in axial piston pump bearings', *ISA Transactions*, Vol. 88, pp.86–198.

Wang, S., Yub, J., Lapirac, E. et al. (2013) 'A modified support vector data description based novelty detection approach for machinery components', *Applied Soft Computing*, Vol. 13, No. 2, pp.1193–1205.

Wei, X., Chao, Q., Tao, J. et al. (2021) 'Cavitation fault diagnosis method for high-speed plunger pump based on LSTM and CNN', *Acta Aeronautica et Astronautica Sinica*, Vol. 42, No. 3, pp.435–445.

Wiens, T, Fernandes, J. (2019) 'Application of data reduction techniques to dynamic condition monitoring of an axial piston pump', in *Proceedings of the ASME/BATH 2019 Symposium on Fluid Power and Motion Control*, Longboat Key, USA, V001T01A041.

Wu, Z., Xiao, C., Tang, H. et al. (2021) 'Fault diagnosis of axial piston pump based on polynomial chirplet transform and variational mode decomposition under variable speed conditions', *Chinese Hydraulics and Pneumatics*, Vol. 45, No. 7, pp.77–82.

Załuski, P. (2022) 'Influence of fluid compressibility and movements of the swash plate axis of rotation on the volumetric efficiency of axial piston pumps', *Energies*, Vol. 15, No. 1, p.298.

Zhang, L., Qiao, F., Wang, J. et al. (2021) 'Equipment health assessment based on improved incremental support vector data description', *IEEE Transactions on Systems, Man, and Cybernetics: Systems*, Vol. 51, No. 5, pp.3205–3216.